

UDC 621-033.6:669.018.9; 621-033.6:666.1/7; 621-033.6:666.1

DOI dx.doi.org/10.17073/1997-308X-2022-3-45-54

## Fabrication and oxidation resistance of the non-stoichiometric tantalum-hafnium carbonitride

© 2022 г. **V.S. Suvorova, A.A. Nepapushev, D.O. Moskovskikh, K.V. Kuskov**

National University of Science and Technology (NUST) «MISIS», Moscow, Russia

Received 14.04.2022, revised 21.04.2022, accepted for publication 29.04.2022

**Abstract:** This research was conducted to obtain non-stoichiometric tantalum-hafnium carbonitride powder of the  $Fm3m$  (225) structural type using a combination of mechanical activation (MA) and self-propagating high-temperature synthesis (SHS) methods. Mechanical activation for 60 min in a low-energy mode (347 rpm) forms Ta/Hf/C composite particles 1 to 20  $\mu\text{m}$  in size with a layered structure and contributes to a uniform distribution of elements. SHS of a mechanically activated Ta + Hf + C mixture in a nitrogen atmosphere (0.8 MPa) leads to the formation of a single-phase tantalum-hafnium carbonitride powder with the  $\text{Ta}_{0.25}\text{Hf}_{0.75}\text{C}_{0.5}\text{N}_{0.3}$  composition where particles feature by a «spongy» morphology with pores and caverns and consist of submicron grains. Spark plasma sintering (SPS) was used to obtain a bulk sample of tantalum-hafnium carbonitride with a grain size of 3 to 5  $\mu\text{m}$ , relative density of  $98.2 \pm 0.3\%$ , hardness of  $19.8 \pm 0.2$  GPa, and crack resistance of  $5.4 \pm 0.4$  MPa·m<sup>1/2</sup>. The kinetics of (Ta,Hf)CN oxidation at 1200 °C in air is described by a parabolic law suggesting the formation of an  $\text{Hf}_6\text{Ta}_2\text{O}_{17} + m\text{HfO}_2$  oxide layer with a low oxygen diffusion rate where the oxidation rate is 0.006 mg/(cm<sup>2</sup>·s). A (Ta,Hf)CN oxidation mechanism is proposed, which states that  $\text{Ta}_2\text{O}_5$  and  $\text{HfO}_2$  are formed on the surface of grains at the first stage that react with each other at the second stage to form a  $\text{Hf}_6\text{Ta}_2\text{O}_{17}$  homologous superstructure and monoclinic  $\text{HfO}_2$ . CO, CO<sub>2</sub>, NO and NO<sub>2</sub> gaseous oxidation products are released with the formation of pores and cracks.

**Keywords:** carbonitride, mechanical activation, self-propagating high-temperature synthesis (SHS), ceramics, spark plasma sintering (SPS), oxidation resistance.

**Suvorova V.S.** – Postgraduate student, Department of powder metallurgy and functional coatings, Engineer of the scientific project of the Science and Research Center (SRC) «Functional nanoceramic», National University of Science and Technology (NUST) «MISIS» (119049, Russia, Moscow, Leninskiy pr., 4). E-mail: buynevich.vs@misis.ru.

**Nepapushev A.A.** – Cand. Sci. (Eng.), Senior researcher, SRC «Functional nanoceramic», NUST «MISIS». E-mail: anepapushev@gmail.com.

**Moskovskikh D.O.** – Cand. Sci. (Eng.), Director of SRC «Functional nanoceramic», NUST «MISIS». E-mail: mos@misis.ru.

**Kuskov K.V.** – Research scientist, SRC «Functional nanoceramic», NUST «MISIS». E-mail: kkuskov@misis.ru.

**For citation:** Suvorova V.S., Nepapushev A.A., Moskovskikh D.O., Kuskov K.V. Fabrication and oxidation resistance of the non-stoichiometric tantalum-hafnium carbonitride. *Izvestiya Vuzov. Poroshkovaya Metallurgiya i Funktsional'nye Pokrytiya (Powder Metallurgy and Functional Coatings)*. 2022. Vol. 16. No. 3. P. 45–54 (In Russ.). DOI: dx.doi.org/10.17073/1997-308X-2022-3-45-54.

## Получение нестехиометрического тантал-гафниевого карбонитрида и исследование его окислительной стойкости

**В.С. Суворова, А.А. Непашев, Д.О. Московских, К.В. Кусков**

Национальный исследовательский технологический университет «МИСиС», г. Москва, Россия

Статья поступила в редакцию 14.04.2022 г., доработана 21.04.2022 г., подписана в печать 29.04.2022 г.

**Аннотация:** В данной работе комбинацией методов механического активирования (МА) и самораспространяющегося высокотемпературного синтеза (СВС) получен порошок нестехиометрического тантал-гафниевого карбонитрида.

да структурного типа  $Fm\bar{3}m$  (225). Механическое активирование в течение 60 мин в низкоэнергетическом режиме (347 об/мин) приводит к формированию композиционных частиц Ta/Hf/C слоистой структуры, размер которых варьируется от 1 до 20 мкм, и способствует равномерному распределению элементов. Продуктом СВС механоактивированной смеси Ta + Hf + C в среде азота (0,8 МПа) является однофазный порошок тантал-гафниевого карбонитрида состава  $Ta_{0,25}Hf_{0,75}C_{0,5}N_{0,3}$ , частицы которого характеризуются губчатой морфологией с порами и кавернами и состоят из субмикронных зерен. Посредством искрового плазменного спекания (ИПС) получен объемный образец тантал-гафниевого карбонитрида, размер зерен которого варьируется от 3 до 5 мкм, с относительной плотностью  $98,2 \pm 0,3 \%$ , твердостью  $19,8 \pm 0,2$  ГПа и трещиностойкостью  $5,4 \pm 0,4$  МПа·м<sup>1/2</sup>. Кинетика окисления (Ta,Hf)CN при температуре 1200 °C на воздухе описывается параболическим законом, что свидетельствует о формировании оксидного слоя  $Hf_6Ta_2O_{17} + mHfO_2$  с низкой скоростью диффузии кислорода, скорость окисления при этом составляет 0,006 мг/(см<sup>2</sup>·с). Предложен механизм окисления (Ta,Hf)CN, заключающийся в том, что на первой стадии на поверхности зерен формируются  $Ta_2O_5$  и  $HfO_2$ , которые на второй стадии вступают в реакцию друг с другом с образованием гомологичной сверхструктуры  $Hf_6Ta_2O_{17}$  и моноклинного  $HfO_2$ . Высвобождение газообразных продуктов окисления CO, CO<sub>2</sub>, NO и NO<sub>2</sub> сопровождается образованием пор и трещин.

**Ключевые слова:** карбонитрид, механическое активирование, самораспространяющийся высокотемпературный синтез (СВС), керамика, искровое плазменное спекание (ИПС), окислительная стойкость.

**Суворова В.С.** – аспирант кафедры порошковой металлургии и функциональных покрытий, инженер научного проекта НИЦ «Конструкционные керамические наноматериалы», НИТУ «МИСиС» (119049, г. Москва, Ленинский пр-т, 4). E-mail: buynevich.vs@misis.ru.

**Непапушев А.А.** – канд. техн. наук, ст. науч. сотрудник НИЦ «Конструкционные керамические наноматериалы», НИТУ «МИСиС». E-mail: anepapushev@gmail.com.

**Московских Д.О.** – канд. техн. наук, директор НИЦ «Конструкционные керамические наноматериалы», НИТУ «МИСиС». E-mail: mos@misis.ru.

**Кусков К.В.** – науч. сотрудник НИЦ «Конструкционные керамические наноматериалы», НИТУ «МИСиС». E-mail: kkuskov@misis.ru.

**Для цитирования:** Суворова В.С., Непапушев А.А., Московских Д.О., Кусков К.В. Получение нестехиометрического тантал-гафниевого карбонитрида и исследование его окислительной стойкости. *Известия вузов. Порошковая металлургия и функциональные покрытия*. 2022. Т. 16. № 3. С. 45–54.  
DOI: dx.doi.org/10.17073/1997-308X-2022-3-45-54.

## Introduction

Few of the most advanced materials can withstand intensive mechanical and thermal loads above 2000 °C. The only choice is group IVB and VB transition metal compounds: borides, carbides, and nitrides. Due to the presence of strong covalent and ionic bonds, these materials have high melting temperatures (>2,500 °C), excellent mechanical and thermophysical properties, and chemical and phase stability [1, 2]. Tantalum and hafnium carbides are of special interest among other refractory compounds. They have the highest melting points (3,880 and 3,890 °C, respectively), a higher hardness (~25 GPa), elastic modulus (~450 GPa), and strength (~250 MPa) while thermal conductivity ranges from 20 to 30 W/(m·K) [3–5].

A significant disadvantage of refractory compounds is their relatively low oxidation resistance. Most of them work well in protective atmospheres, while in the air they oxidize intensively at 400–800 °C,

forming porous and cracking oxide films, which cannot protect the base material from further oxidation [6].

There are several approaches to increasing their heat resistance. For example, the addition of SiC to refractory ceramics initiates the formation of a dense MeSiO<sub>4</sub> oxide layer, thus preventing oxygen diffusion to the material [7, 8]. Another approach is to create more complex compounds from refractory transition metal carbides and nitrides. Such solid solutions tend to have enhanced physical, mechanical, and thermophysical properties, and higher oxidation resistance, since refractory oxide films with low oxygen diffusion rates are formed [9]. Savvatimskiy A. et al. [10] showed that the  $Ta_{0,80}Hf_{0,20}C$  melting temperature is 4030 °C. It significantly exceeds the melting temperatures of tantalum and hafnium carbides, the current «record-breakers». Kurbatkina V. et al. [11] demonstrated

that double carbides (Ta, Hf)C and (Ta, Zr)C have a higher hardness and Young's modulus compared to binary compounds.

Among the complex compounds, transition metal carbonitrides are no less interesting in terms of high-temperature applications. Hong Q.J. et al. [12] performed a theoretical analysis and showed that the introduction of nitrogen atoms into the lattice of refractory (Ta, Hf)C increases not only the melting point but also the oxidation resistance. As they reported, for the Ta—Hf—C—N system the tantalum-hafnium carbonitride ( $\text{Hf}_{0.75}\text{Ta}_{0.25}\text{C}_{0.5}\text{N}_{0.25}$ ) has the highest properties. We thus decided to manufacture this compound and analyze its properties.

However, the synthesis of non-stoichiometric compounds is challenging. Conventional technologies produce only  $\text{MeC}_x\text{N}_{1-x}$  stoichiometric phases, since it is not possible to adjust the nitrogen content in the final product. An alternative method for producing a wide range of multicomponent compounds is self-propagating high-temperature synthesis (SHS) [13], as developed by A.G. Merzhanov and I.P. Borovinskaya in 1972. This is a simple, single-stage, and highly efficient process.

This study aims to manufacture (Ta, Hf)CN dense ceramics by means of spark plasma sintering. The raw material is the powder produced by SHS of mechanically agitated activated Ta + Hf + C mixture in a nitrogen environment. Ceramics oxidation resistance was also studied.

## Materials and methods

Hafnium powder HFM-1 (TU 48-4-176-85 (97) specification, particle size  $d \leq 50 \mu\text{m}$ , 98.8 % purity), tantalum powder TaP-1 (TU 1870-258-00196109-01 95.136-69 specification, particle size  $d = 40+60 \mu\text{m}$ , 99.9 % purity) and carbon black P804T (TU 38-1154-88 specification, particle size  $d \leq 0.2 \mu\text{m}$ , 99.5 % purity) were used as precursors. The mechanical milling was performed in an argon environment using a 4.8 Grade argon (GOST 10157-79, 99.993 % purity). The SHS process involved filtration combustion in grade 1 nitrogen (GOST 9293-74, 99.999 % purity).

Before synthesis, the Ta + Hf + C powder mixture (24.3 Ta + 72.1 Hf + 3.6 C wt.%) was mechanically activated in an Activator-2S high-performance plane-

tary ball mill (Activator, Russia). The powder mixture and steel balls (1 : 20 weight mass ratio) were loaded into steel jars filled with argon at 0.6 MPa. Mechanical activation lasted for 60 min at a 347 rpm speed of the jars.

A constant-pressure lab reactor was used for the SHS process. The activated Ta + Hf + C powder mixture was placed loosely on a removable reactor rack. The reactor chamber was evacuated with a fore vacuum pump. Then nitrogen was pumped through a dedicated pipe to a pressure of 0.8 MPa. A self-sustaining exothermic reaction was initiated by briefly applying a voltage to the tungsten coil connected to the power supply.

The SHS powder was consolidated with a Labox 650 spark plasma sintering machine (SinterLand, Japan) in an argon environment at 2000 °C, 50 MPa press pressure, and 20 min. holding time. The heating rate was 100 °C/min.

The microstructure and elemental composition were analyzed with a JSM-7600F scanning electron microscope (JEOL Ltd., Japan) equipped with an INCA SDD 61 X-MAX X-ray microanalysis system (Oxford Instruments, UK) in backscattered electron mode, 15 kV accelerating voltage and 3 nm resolution.

The phase composition of the powders after mechanical activation and SHS and of the sintered samples was studied using a Difrax-401 X-ray diffractometer (Research Instruments, Russia),  $\text{CuK}_\alpha$  radiation, step scanning mode (scanning step: 0.1°) 20° to 100° angle range, 2 s exposure. The ICDD PDF databases were used to analyze the resulting spectra.

The nitrogen and carbon contents in the synthesized powders and sintered samples were determined by carrier gas hot extraction. A TC-600 (Leco, USA) instrument estimated the amount of nitrogen and oxygen in the compounds by IR adsorption (for oxygen) and thermal conductivity (for nitrogen) analysis during the reduction melting of the samples in a resistance furnace in a helium flow. A CS-600 (Leco) instrument was used to measure the carbon content. For this purpose, the samples were subjected to oxidative melting in an induction furnace and the amount of  $\text{CO}_2$  released was measured by IR absorption.

The density of compacted ceramic materials was determined by hydrostatic weighing under GOST 20018-74 [14]. At least 10 measurements were taken in air and distilled water ( $\rho_w = 0.9978 \text{ g/cm}^3$ ). A layer of vaseline

( $\rho_v = 0.870 \text{ g/cm}^3$ ) was applied to cover the open pores. We applied an ES 220A analytical balance (Precisa, Switzerland),  $\pm 0.0001 \text{ g}$  accuracy.

A Micro-Hardness Tester (CSM Instruments, Switzerland) was used to measure Young's modulus ( $E$ ) at a 100 mN applied load.

We used a Durascan 70 hardness testing machine (Struers ApS, Denmark) to estimate the hardness and crack resistance of the consolidated materials by the Vickers method, GOST 2999-75 [15]. A max load of 9.8 kg was applied for 20 s. After the load was removed, the diagonals of the imprint on the sample surface and the crack lengths were measured. At least 10 measurements were taken with each sample. The software evaluated the hardness automatically. We used the Anstis equation to assess the fracture toughness:

$$K_{Ic} = 0,016 \left( \frac{E}{HV} \right)^{1/2} \frac{P}{c^{3/2}}, \quad (1)$$

wherein  $E$  is Young's modulus, GPa;  $HV$  is the hardness, GPa;  $P$  is the applied load, N;  $c$  is the crack length from the center of the imprint to the crack end, m.

We used an SSHOL 1.1,6/12-M3 electric furnace (Tula-Therm, Russia) at 1200 °C for 180 min to study the chemical kinetics and oxidation of a box-shaped (Ta, Hf)CN shape. The samples were measured using a micrometer. Before the analysis, the samples were polished on a Tegramin grinding and polishing system (Struers, Denmark). The sample was placed on a platform in the furnace in an alundum crucible. The degree of oxidation was assessed after 5, 10, 15, 20, 30, 60, 120, and 180 min using the gravimetric method. We measured the weight gain using a GR-202 analytical balance (AND, Japan),  $10^{-4} \text{ g}$  accuracy. Before weighing, the samples and with crucibles were cooled to room temperature.

## Results and discussion

Mechanical activation (MA) is an important step before SHS. It enhances reactivity and helps control the microstructure of the combustion products [16]. Fig. 1 shows that the MA of tantalum, hafnium, and carbon powders (Ta + Hf + C) for 60 min resulted in formation of composite Ta/Hf/C particles ranging from 1 to 20  $\mu\text{m}$ . A detailed examination of their cross sections identified the layers (Fig. 1, *b* and *c*) corresponding to

heavy (Ta and Hf: light areas) and light (C: dark areas) elements.

Fig. 2 shows the (Ta, Hf)CN microstructure after SHS of a mechanically activated Ta + Hf + C mixture in a nitrogen environment. The morphology of SHS powder particles (Fig. 2, *a*) is identical to that of the composite Ta/Hf/C particles after MA (see Fig. 1, *a*). Cross-sectional analysis of (Ta, Hf)CN particles discovered pores and caverns. A more detailed examination revealed melted grains from 1 to 3  $\mu\text{m}$  (Fig. 2, *b*). This can be explained by hafnium and tantalum melting during combustion (adiabatic combustion temperature  $t_{ad} = 3073 \text{ }^\circ\text{C}$ ) and the formation of (Ta, Hf)CN through the liquid phase. As Fig. 2, *c* shows, Ta, Hf, C, and N are evenly distributed after SHS.

Chemical analysis indicated that the SHS powder contains 3.7 wt.% C and 2.2 wt.% N, which corresponds to  $\text{Hf}_{0.75}\text{Ta}_{0.25}\text{C}_{0.5}\text{N}_{0.25}$ . It should be noted that the oxygen content does not exceed 0.8 wt. %.

Fig. 3 shows the sample XRD patterns after SHS and spark plasma sintering (SPS). The crystal structure of the sintered (Ta, Hf)CN substance is identical to that of the synthesized powder. Its space group is  $Fm\bar{3}m$  (225). However, after sintering, the main phase peaks became more symmetrical, indicating a homogenization of the chemical composition across the sample during SPS. The (Ta, Hf)CN lattice parameter after SHS and SPS is 0.455 nm. This is between HfC (0.464 nm) and HfN (0.453 nm). The value we obtained is higher than that for TaC (0.446 nm) and TaN (0.434 nm). In both cases, the XRD patterns show  $\text{HfO}_2$  peaks of the  $P42/nmc$  (14) space group.

Fig. 4 shows a typical microstructure of the sample after sintering. The grain size of the main (Ta, Hf)CN phase (light areas) varies from 3 to 5  $\mu\text{m}$ , with small  $\text{HfO}_2$  inclusions (dark gray areas) at their boundaries. The sintered (Ta, Hf)CN powder has a  $98.2 \pm 0.3 \%$  relative density and high mechanical properties (hardness  $H = 19.8 \pm 0.2 \text{ GPa}$ , Young's modulus  $E = 570 \pm 20 \text{ GPa}$ , fracture toughness  $K_{Ic} = 5.4 \pm 0.4 \text{ MPa} \cdot \text{m}^{1/2}$ ). This is comparable to the properties of similar materials [11, 17–19].

We studied the kinetics and oxidation mechanism of the  $\text{Hf}_{0.75}\text{Ta}_{0.25}\text{C}_{0.5}\text{N}_{0.25}$  using a muffle electric furnace at 1200 °C for 180 min. Fig. 5 shows the kinetic curve of the sample mass change. The oxidation of tantalum-hafnium carbonitride follows a parabo-

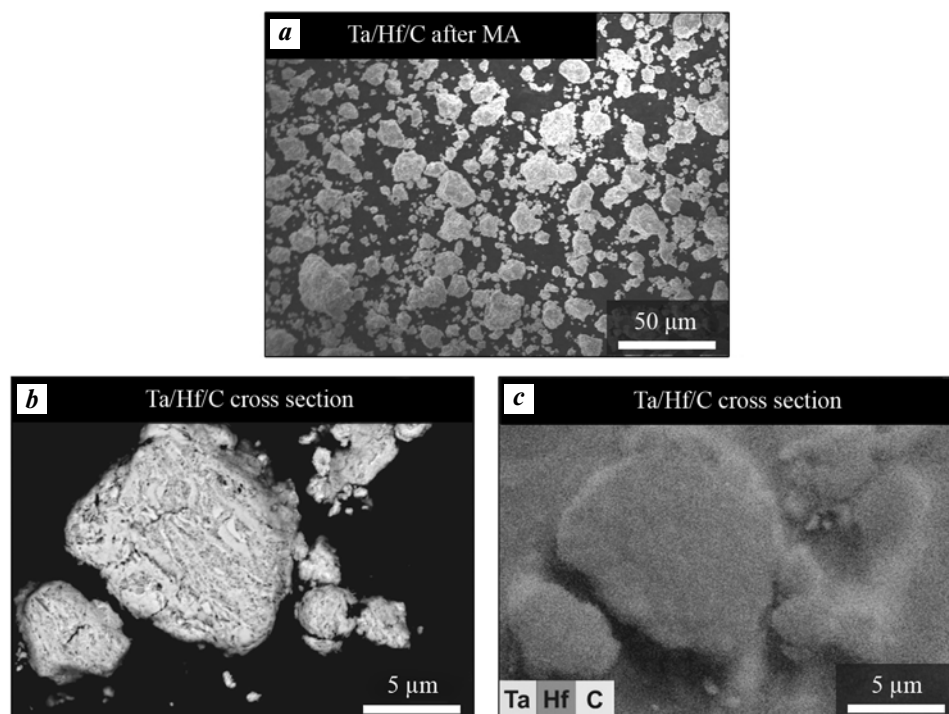


**Fig. 1.** Micrograph (a), cross section (b) of Ta/Hf/C composite particles and map of element distribution after mechanical activation (c)

**Рис. 1.** Микрофотография (a), поперечное сечение (b) композиционных частиц Ta/Hf/C и карта распределения элементов после механического активирования (c)

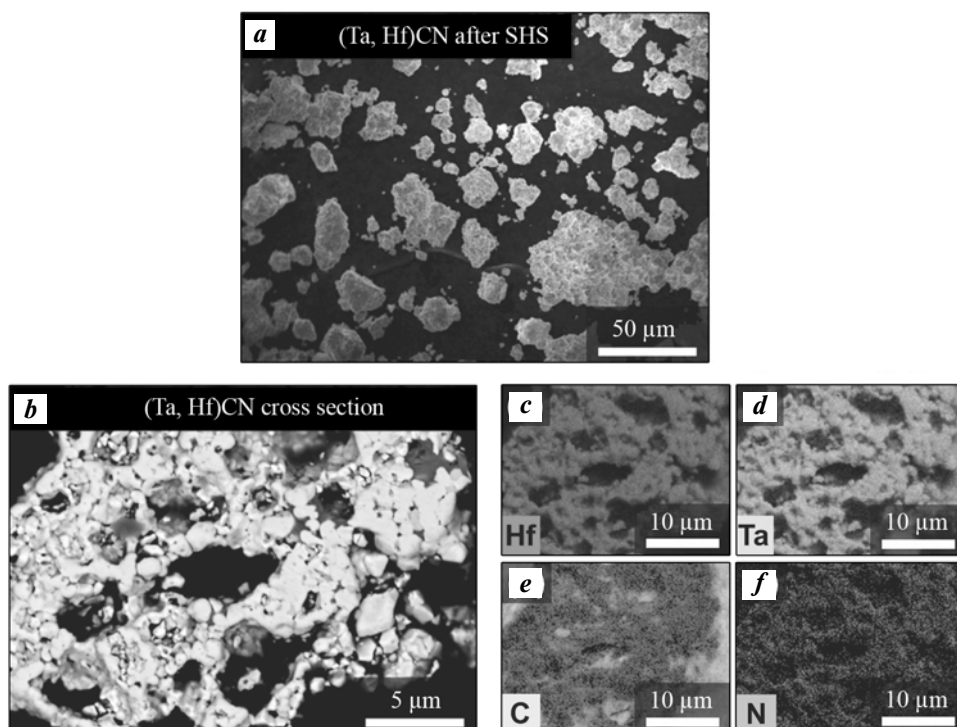


**Fig. 2.** Micrograph (a), cross section (b) of (Ta,Hf)CN particles and distribution of elements after SHS (c–f)

**Рис. 2.** Микрофотография (a), поперечное сечение (b) частиц (Ta,Hf)CN и распределение элементов после СВС (c–f)

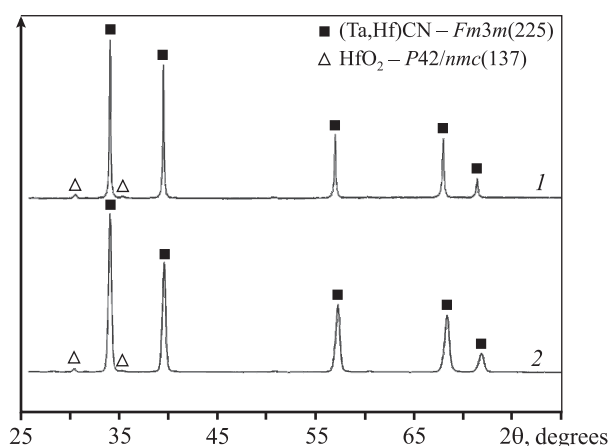


**Fig. 3.** XRD patterns of (Ta,Hf)CN samples after SPS (1) and SHS (2)

**Рис. 3.** Дифрактограммы образцов (Ta,Hf)CN после ИПС (1) и СВС (2)

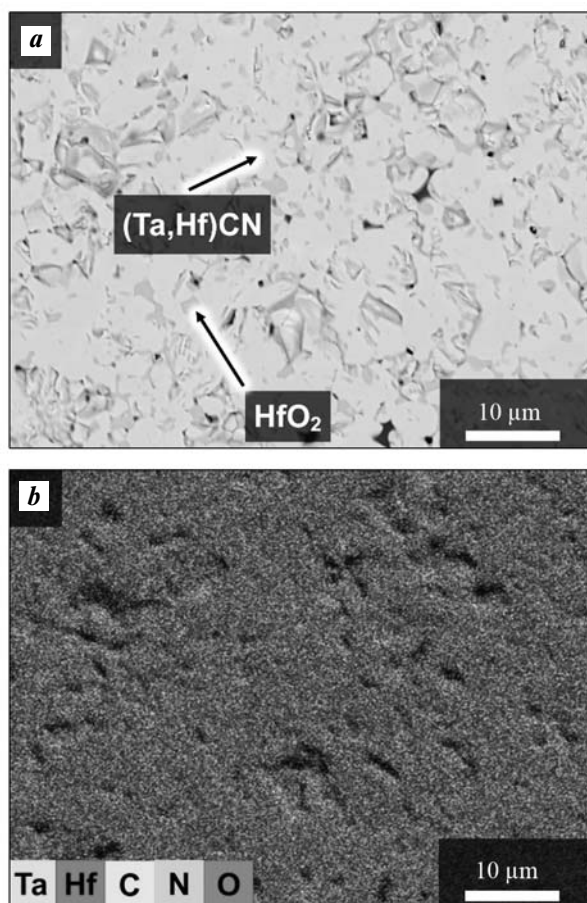


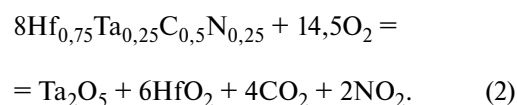
**Fig. 4.** Microstructure of sample (Ta,Hf)CN (a) and map of element distribution after SPS (b)

**Рис. 4.** Микроструктура образца (Ta,Hf)CN (a) и карта распределения элементов после ИПС (b)

lic law. Between 0 and 30 minutes, the max oxidation rate was  $0.012 \text{ mg}/(\text{cm}^2 \cdot \text{s})$ ; as the oxide layer grew, it decreased to  $0.004 \text{ mg}/(\text{cm}^2 \cdot \text{s})$ . The average oxidation rate was  $\sim 0.006 \text{ mg}/(\text{cm}^2 \cdot \text{s})$  and the weight gain was  $62 \text{ mg}/\text{cm}^2$ .

As Fig. 6 shows, a dense oxide layer is formed on the surface of the  $\text{Hf}_{0.75}\text{Ta}_{0.25}\text{C}_{0.5}\text{N}_{0.25}$  sample after oxidation. XRD indicated (Fig. 7) that it consists of two phases: monoclinic  $\text{HfO}_2$ ,  $P21/c(14)$  space group; and the  $\text{Hf}_6\text{Ta}_2\text{O}_{17}$  orthorhombic superstructure ( $Ima2(46)$ ). The intensity of the complex oxide peaks is much greater than that of hafnium oxide. It indicates the predominance of  $\text{Hf}_6\text{Ta}_2\text{O}_{17}$  in the oxide layer.

Based on the results presented in this work and the literature [24], we may assume the following oxidation process (Fig. 8). Initially,  $\text{Ta}_2\text{O}_5$  and  $\text{HfO}_2$  are formed on the surface of (Ta, Hf)CN grains as result of the reaction



The  $\text{Hf}_{0.75}\text{Ta}_{0.25}\text{C}_{0.5}\text{N}_{0.25}$  compound has a high Hf content, so mainly  $\text{HfO}_2$  is formed on the surface of the particles. Since the Gibbs energy for the  $\text{Ta}_2\text{O}_5$  formation ( $\Delta G = -72 \text{ kJ/mol}$  [20]) is more negative when compared to that for  $\text{HfO}_2$  ( $\Delta G = -1088 \text{ kJ/mol}$  [21]),  $\text{Ta}_2\text{O}_5$  is most probably located at the surface of

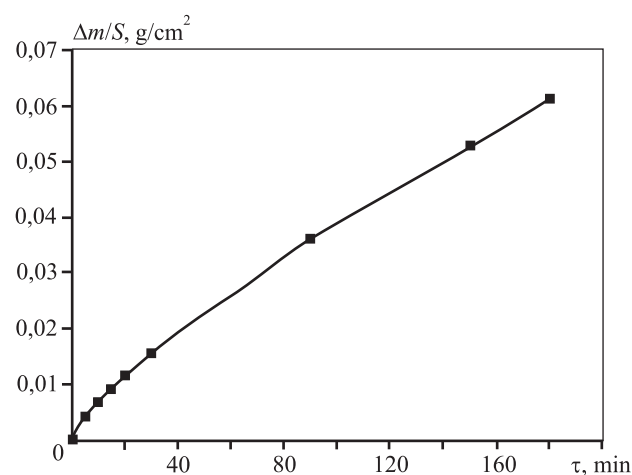


**Fig. 5.** Kinetic curve of (Ta,Hf)CN sintered sample oxidation

**Рис. 5.** Кинетическая кривая окисления спеченного образца (Ta,Hf)CN



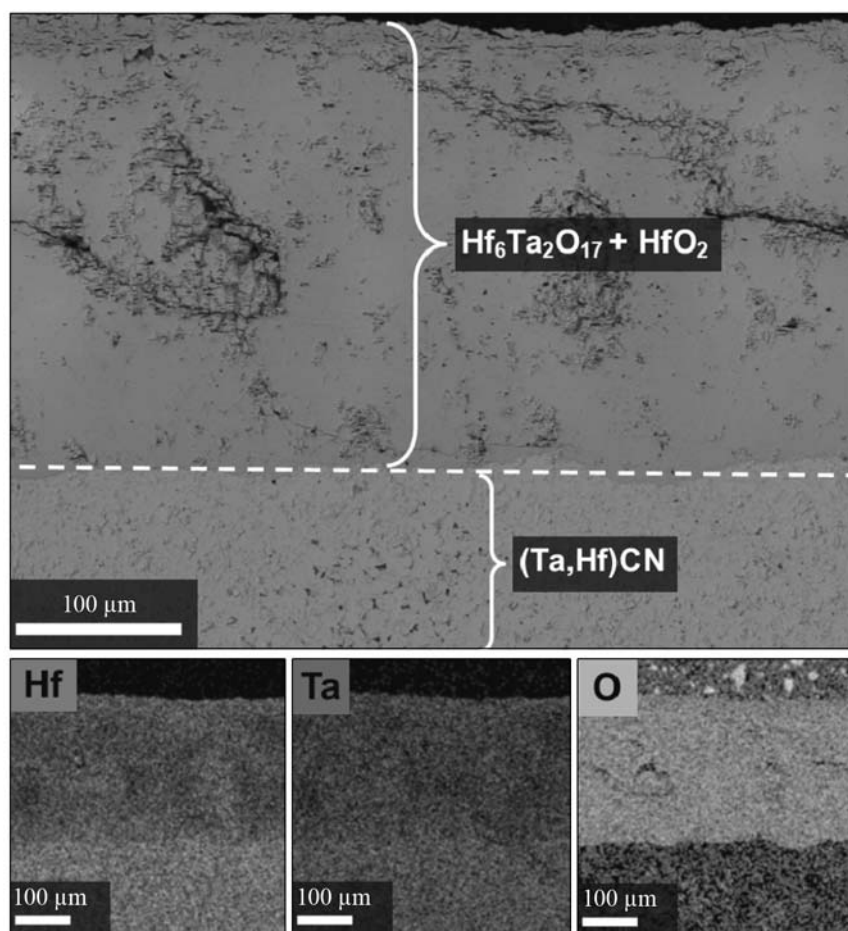


**Fig. 6.** Micrograph of (Ta,Hf)CN cross section after oxidation at  $t = 1200\text{ }^{\circ}\text{C}$  and distribution of elements in oxide layer

**Рис. 6.** Микрофотография поперечного сечения образца (Ta,Hf)CN после окисления при  $t = 1200\text{ }^{\circ}\text{C}$  и распределение элементов в оксидном слое

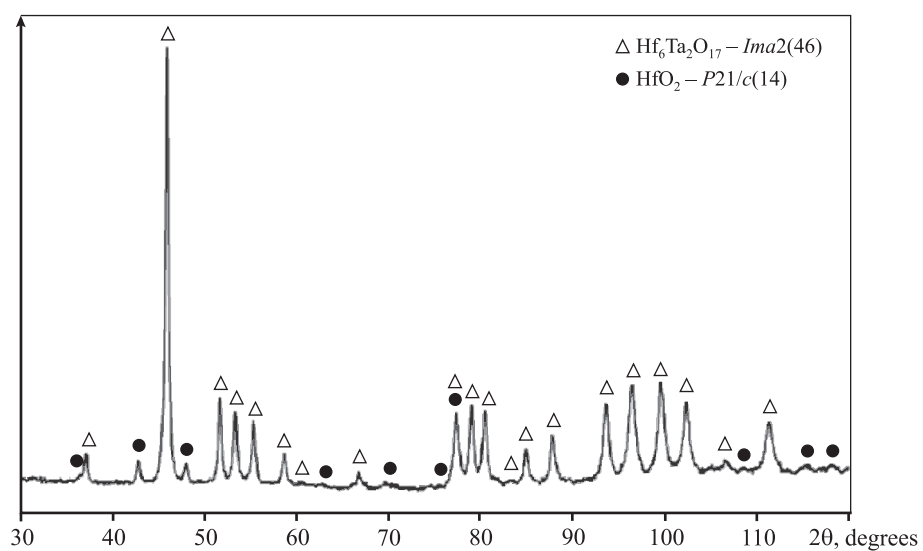


**Fig. 7.** XRD pattern of (Ta,Hf)CN oxide layer

**Рис. 7.** Дифрактограмма оксидного слоя (Ta,Hf)CN

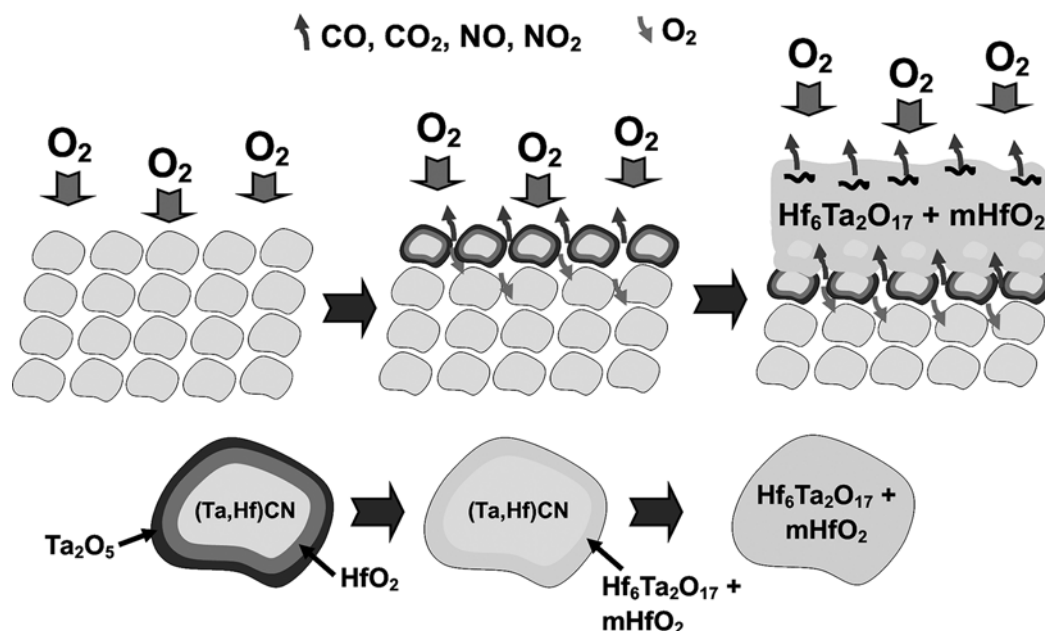
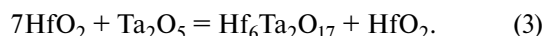


Fig. 8. (Ta,Hf)CN oxidation mechanism

Рис. 8. Механизм окисления (Ta,Hf)CN

HfO<sub>2</sub>, as shown in Fig. 8. The phase diagram [22] indicates that HfO<sub>2</sub> and Ta<sub>2</sub>O<sub>5</sub> oxides mutually react at  $t = 1200$  °C to form Hf<sub>6</sub>Ta<sub>2</sub>O<sub>17</sub> and a monoclinic HfO<sub>2</sub> substance:



Gaseous CO<sub>2</sub> and NO<sub>2</sub> are generated during the (Ta, Hf)CN oxidation (reaction (2)). The gases pass through the oxide layer, forming pores and cracks.

From studies [23, 24] we can conclude that Hf<sub>6</sub>Ta<sub>2</sub>O<sub>17</sub> as an oxide layer has a lower oxygen diffusion rate compared to HfO<sub>2</sub>, high density, and adhesion to the substrate. It explains the relatively low oxidation rate of (Ta, Hf)CN.

## Conclusion

An SHS process applied to a mechanically activated Ta + Hf + C mixture produces a Hf<sub>0.75</sub>Ta<sub>0.25</sub>C<sub>0.5</sub>N<sub>0.25</sub> single-phase non-stoichiometric tantalum-hafnium carbonitride powder. Mechanical activation contributed to the uniform distribution of elements and the formation of composite Ta/Hf/C particles. SHS produces spongy particles consisting of submicron grains.

The SPS process at  $t = 2000$  °C, 50 MPa and 20 min holding time produces bulk tantalum-hafnium carboni-

tride with  $98.2 \pm 0.3$  % relative density,  $19.8 \pm 0.2$  GPa hardness,  $570 \pm 20$  GPa Young's modulus, and  $5.4 \pm 0.4$  MPa·m<sup>1/2</sup> fracture toughness. The mechanical properties of the resulting ceramics are higher than those of binary compounds. They are comparable to double carbides.

The tantalum-hafnium carbonitride demonstrated high oxidation resistance (0.006 mg/(cm<sup>2</sup>·s)) at  $t = 1,200$  °C in the air. The oxidation kinetics follows the parabolic law. This can be explained by the formation of an oxide film with a low oxygen diffusion rate. The film consists of the Hf<sub>6</sub>Ta<sub>2</sub>O<sub>17</sub> homologous superstructure and the HfO<sub>2</sub> monoclinic substance.

**Acknowledgments:** The research was funded by Russian Science Foundation Grant № 19-79-10280.

Работа выполнена при финансовой поддержке гранта РФФ № 19-79-10280.

## References

1. Fahrenholtz W.G., Wuchina E.J., Lee W.E., Zhou Y. Ultra-high temperature ceramics: materials for extreme environment applications. N.Y.: John Wiley & Sons, 2014.
2. Vorotilo S., Sidnov K., Kurbatkina V.V., Loginov P.A., Patsera E.I., Sviridova T.A., Lobova T.A., Levashov E.A., Klechkovskaya V.V. Super-hardening and localized



- plastic deformation behaviors in  $\text{ZrB}_2\text{—TaB}_2$  ceramics. *J. Alloys Compd.* 2022. Vol. 901. P. 163368. DOI: 10.1016/j.jallcom.2021.163368.
3. Ushakov S.V., Navrotsky A., Hong Q. J., van de Walle A. Carbides and nitrides of zirconium and hafnium. *Materials*. 2019. Vol. 12. Iss. 17. P. 2728. DOI: 10.3390/ma12172728.
  4. Sheindlin M., Falyakhov T., Petukhov S., Valyano G., Vasin A. Recent advances in the study of high-temperature behaviour of non-stoichiometric  $\text{TaC}_x$ ,  $\text{HfC}_x$  and  $\text{ZrC}_x$  carbides in the domain of their congruent melting point. *Adv. Appl. Ceram.* 2018. Vol. 117. Iss. 1. P. s48—s55. DOI: 10.1080/17436753.2018.1510819.
  5. Aritonang S., Ezha Kurniasari W. S., Juhana R., Herawan T. Analyzing tantalum carbide (TaC) and hafnium carbide (HfC) for spacecraft material. In: *Recent trends in manufacturing and materials towards industry 4.0*. Singapore, Springer, 2021. P. 925—933. DOI: 10.1007/978-981-15-9505-9\_81.
  6. Shimada S. Interfacial reaction on oxidation of carbides with formation of carbon. *Solid State Ionics*. 2001. Vol. 141. P. 99—104. DOI: 10.1016/S0167-2738(01)00727-5.
  7. Sevastyanov V.G., Simonenko E.P., Gordeev A.N., Simonenko N.P., Kolesnikov A.F., Papynov E.K., Shichalin O.O., Avramenko V.A., Kuznetsov N.T. Behavior of a sample of the ceramic material  $\text{HfB}_2\text{—SiC}$  (45 vol.%) in the flow of dissociated air and the analysis of the emission spectrum of the boundary layer above its surface. *Russ. J. Inorg. Chem.* 2015. Vol. 60. Iss. 11. P. 1360—1373. DOI: 10.1134/S0036023615110133.
  8. Potanin A.Yu., Astapova A.N., Pogozhev Yu.S., Rupasov S.I., Shvyndina N.V., Klechkovskaya V.V., Levashov E.A., Timofeev I.A., Timofeev A.N. Oxidation of  $\text{HfB}_2\text{—SiC}$  ceramics under static and dynamic conditions. *J. Eur. Ceram. Soc.* 2021. Vol. 41. Iss. 16. P. 34—47. DOI: 10.1016/j.jeurceramsoc.2021.09.018.
  9. Zhang C., Boesl B., Agarwal A. Oxidation resistance of tantalum carbide-hafnium carbide solid solutions under the extreme conditions of a plasma jet. *Ceram. Int.* 2017. Vol. 43. Iss. 17. P. 14798—14806. DOI: 10.1016/j.ceramint.2017.07.227.
  10. Savvatimskiy A.I., Onufriev S.V., Muboyadzhyan S.A. Thermophysical properties of the most refractory carbide  $\text{Ta}_{0.8}\text{Hf}_{0.2}\text{C}$  under high temperatures (2000—5000 K). *J. Eur. Ceram. Soc.* 2019. Vol. 39. Iss. 4. P. 907—914. DOI: 10.1016/j.jeurceramsoc.2018.11.030.
  11. Kurbatkina V.V., Patsera E.I., Levashov E.A., Vorotilo S. SHS processing and consolidation of Ta—Ti—C, Ta—Zr—C, and Ta—Hf—C carbides for ultra-high-temperatures application. *Adv. Eng. Mater.* 2018. Vol. 20. Iss. 8. P. 1701075. DOI: 10.1002/adem.201701075.
  12. Hong Q.J., Van De Walle A. Prediction of the material with highest known melting point from ab initio molecular dynamics calculations. *Phys. Rev. B*. 2015. Vol. 92. Iss. 2. P. 020104. DOI: 10.1103/PhysRevB.92.020104.
  13. Сеплярский Б.С., Брауэр Г.Б., Тарасов А.Г. Закономерности горения «безгазовой» системы  $\text{Ti} + 0,5\text{C}$  в спутном потоке азота. *Физика горения и взрыва*. 2011. No. 3. С. 52—59.
  14. Seplyarskii B.S., Brauer G.B., Tarasov A.G. Combustion of the gasless system  $\text{Ti} + 0.5\text{C}$  in a nitrogen coflow. *Fizika goreniya i vzryva*. 2011. Vol. 3. P. 52—59 (In Russ.).
  15. ГОСТ 20018-74 (СТ СЭВ 1253-78, ИСО 3369-75) Сплавы твердые спеченные. Метод определения плотности (с изменениями № 1, 2, 3). М.: Изд-во стандартов, 1991.
  16. GOST 20018-74 (ST SEV 1253-78, ISO 3369-75) Sintered hard alloys. Density determination method. Moscow: Izdatel'stvo standartov, 1991 (In Russ.).
  17. ГОСТ 2999—75. Металлы и сплавы. Метод измерения твердости по Виккерсу (с изм. 1, 2). Управление стандартизации и сертификации сырья и материалов. Изд-во стандартов, 1986.
  18. GOST 2999—75. Metals and alloys. Vickers hardness measurement method. reissue. Management of standardization and certification of raw materials and materials. Moscow: Izdatel'stvo standartov, 1986 (In Russ.).
  19. Mukasyan A.S., Rogachev A.S. Combustion synthesis: mechanically induced nanostructured materials. *J. Mater. Sci.* 2017. Vol. 52. P. 11826—11833. DOI: 10.1007/s10853-017-1075-9.
  20. Ghaffari S.A., Faghihi-Sani M.A., Golestani-Fard F., Mandal H. Spark plasma sintering of TaC—HfC UHTC via disilicides sintering aids. *J. Eur. Ceram. Soc.* 2013. Vol. 33. Iss. 8. P. 1479—1484. DOI: 10.1016/j.jeurceramsoc.2013.01.017.
  21. Cedillos-Barraza O., Grasso S., Al Nasiri N., Jayaseelan D.D., Reece M.J., Lee W.E. Sintering behaviour, sol-

- id solution formation and characterisation of TaC, HfC and TaC—HfC fabricated by spark plasma sintering. *J. Eur. Ceram. Soc.* 2016. Vol. 36. Iss. 7. P. 1539—1548. DOI: 10.1016/j.jeurceramsoc.2016.02.009.
19. Zhang C., Gupta A., Seal S., Boesl B., Agarwal A. Solid solution synthesis of tantalum carbide—hafnium carbide by spark plasma sintering. *J. Amer. Ceram. Soc.* 2017. Vol. 100. Iss. 5. P. 1853—1862. DOI: 10.1111/jace.14778.
20. Ivanov M.V., Perevalov T.V., Aliev V.S., Gritsenko V.A., Kaichev V.V. Electronic structure of  $\delta$ -Ta<sub>2</sub>O<sub>5</sub> with oxygen vacancy: ab initio calculations and comparison with experiment. *J. Appl. Phys.* 2011. Vol. 110. Iss. 2. P. 024115. DOI: 10.1063/1.3606416.
21. Fang Q., Zhang J.-Y., Wang Z., Modreanu M., O'Sullivan B.J., Hurley P.K., Leedham T.L., Hywel D., Audier M.A., Jimenez C., Senateur J.-P. Ian W. Boyda. Interface of ultrathin HfO<sub>2</sub> films deposited by UV-photo-CVD. *Thin Solid Films.* 2004. Vol. 453. P. 203—207. DOI: 10.1016/j.tsf.2003.11.186.
22. McCormack S.J., Tseng K.P., Weber R.J., Kapush D., Ushakov S.V., Navrotsky A., Kriven W.M. In-situ determination of the HfO<sub>2</sub>—Ta<sub>2</sub>O<sub>5</sub>-temperature phase diagram up to 3000 °C. *J. Amer. Ceram. Soc.* 2019. Vol. 102. Iss. 11. P. 7028—7030. DOI: 10.1111/jace.16271.
23. Yang Y., Perepezko J. H., Zhang C. Oxidation synthesis of Hf<sub>6</sub>Ta<sub>2</sub>O<sub>17</sub> superstructures. *Mater. Chem. Phys.* 2017. Vol. 197. P. 154—162. DOI: 10.1016/j.matchemphys.2017.04.055.
24. Zhang C., Boesl B., Agarwal A. Oxidation resistance of tantalum carbide-hafnium carbide solid solutions under the extreme conditions of a plasma jet. *Ceram. Int.* 2017. Vol. 43. Iss. 17. P. 14798—14806. DOI: 10.1016/j.ceramint.2017.07.227.